Phase transitions and the role of vanadium t_{2g} states in $AV_{13}O_{18}$ (A=Sr,Ba)

M. Ikeda,[1] Y. Nagamine,[2] S. Mori,[2] J. E. Kim,[3] K. Kato,[3,4] M. Takata,[3,4] and T. Katsufuji[1,5,6,*]
[1]*Department of Physics, Waseda University, Tokyo 169-8555, Japan*
[2]*Department of Materials Science, Osaka Prefecture University, Sakai 599-8531, Japan*
[3]*Japan Synchrotron Radiation Research Institute, Hyogo 679-5198, Japan*
[4]*RIKEN SPring-8 Center, Hyogo 679-5148, Japan*
[5]*Kagami Memorial Laboratory for Material Science and Technology, Waseda University, Tokyo 169-0051, Japan*
[6]*PRESTO, Japan Science and Technology Corporation, Saitama 332-0012, Japan*
(Received 30 June 2010; revised manuscript received 17 August 2010; published 10 September 2010)

We studied $AV_{13}O_{18}$ (A=Sr,Ba), in which V ions form a face-centered-cubic lattice with periodically missing ions. It was found that there is a phase transition in both $SrV_{13}O_{18}$ (T_c=270 K) and $BaV_{13}O_{18}$ (T_c=200 K), where anomalies are observed in resistivity and magnetic susceptibility. Resistivity shows a contrasting behavior in the low-temperature phase between $SrV_{13}O_{18}$ (a metallic behavior) and $BaV_{13}O_{18}$ (an insulating behavior). By synchrotron x-ray powder-diffraction measurement, it was found that V trimerization occurs at the phase transition of $SrV_{13}O_{18}$. On the other hand, $BaV_{13}O_{18}$ does not show a large change in the x-ray powder diffraction but superlattice peaks at $(0\frac{1}{2}\frac{1}{2})$ was observed in the electron diffraction. Possible orbital states of the t_{2g} electrons in the V ions are discussed.

DOI: 10.1103/PhysRevB.82.104415 PACS number(s): 75.25.Dk, 71.30.+h, 61.50.Ks

I. INTRODUCTION

It is known that orbital degrees of freedom give rise to various types ordered states in transition-metal oxides. This degree of freedom originates from d orbitals with five energetically degenerate levels in the atomic state. Some of the degeneracy is lifted in the crystal but a part of the degeneracy often survives even in the crystal. In this case, localized electrons can choose which of the energetically degenerate states to occupy. This orbital degree of freedom is analogous to the spin degree of freedom of electrons, which can be similarly described in such a way that electron can choose energetically degenerate spin directions, upward or downward.

In some compounds, the orbital degrees of freedom order at low temperatures. This means that, as is the case for spin degrees of freedom, the orbital occupation at neighboring sites has a correlation, and the electrons occupy the same orbital at all the sites (ferro-orbital ordering) or occupy a different orbital at neighboring sites (antiferro-orbital ordering) at low temperatures, depending on the sign of the correlation. The ordering of orbitals and spins are often correlated, and sometimes both order simultaneously,

A large number of orbital orderings with different ordering patterns have been reported so far. For example, $LaMnO_3$ shows an antiferro-orbital ordering below ~700 K, where an electron of the Mn^{3+} ion ($3d^4$) occupies the $3x^2-r^2$ and the $3y^2-r^2$ state alternately.[1] Another example is seen in $LiVO_2$, in which V "trimers" are formed below 500 K. In this V trimer, xy, yz, or zx orbitals form a bond at each side of the V triangles (trimers), and there are three bonding states per trimer, which can accommodate six electrons supplied by three V^{3+} ions ($3d^2$) in a spin-singlet state.[2] There are several differences between the orbital ordering in $LaMnO_3$ and $LiVO_2$: in $LaMnO_3$, electrons exist at each "site" whereas in $LiVO_2$, electrons exist at each "bond." Furthermore, in $LaMnO_3$, the electron with an orbital degree of freedom also has a spin degree of freedom whereas in $LiVO_2$, the spin degrees of freedom are suppressed by the spin-singlet bond formation.

Recent studies have shown that such spin-singlet trimers are common building blocks for the V^{3+} ($3d^2$) ions on the triangle-based lattice. For example, in $SrV_8Ga_4O_{19}$, V trimers are formed on the V^{3+} kagome lattice.[3] In $BaV_{10}O_{15}$ (Refs. 4 and 5) or $Ba_2V_{13}O_{22}$,[6] which are composed of the bilayer ($BaV_{10}O_{15}$) or trilayer ($Ba_2V_{13}O_{22}$) slab of the V ions on the face-centered-cubic (fcc) lattice with periodically missing ions, three-dimensional V trimer network was observed.

In this paper, we show that $SrV_{13}O_{18}$ is another compound showing V trimerization. On the other hand, $BaV_{13}O_{18}$, which takes the same crystal structure as that of $SrV_{13}O_{18}$, shows a different ordered phase at low temperatures.

$AV_{13}O_{18}$ (A=Sr,Ba) was first synthesized by Iwasaki *et al.*[7,8] The crystal structure is based on VO in the sodium-chloride structure; all the V ions are on the fcc lattice.[7,8] As is well known, the fcc lattice can be regarded as the stacking of the triangular lattices with the ABCABC… periodicity along the diagonal direction. In $AV_{13}O_{18}$, there are periodically missing ions from such a triangular lattice of the V ions and as shown in Fig. 1, the lattice as a result can be regarded as the V "stars" made of 13 V ions (surrounded by a dashed circle in Fig. 1), which are connected to each other at their pointed tips. There are three inequivalent V ions in this crystal structure, one center ion (V1), six ions surrounding the center ion (V3), and six ions at the pointed tips of the star (V2). Along the c axis (perpendicular to the plane), not only the position of the triangular lattice but also the position of the center ion (V1) shifts with the ABCABC… periodicity. The symmetry of the crystal is trigonal but since the direction of the primitive vector for the unit cell is not parallel to the primitive vector of the triangular lattice (see Fig. 1), the crystal has no other symmetry operations than the threefold rotation and inversion. The O ions also form a fcc lattice with periodically missing ions, and the A ion replaces the

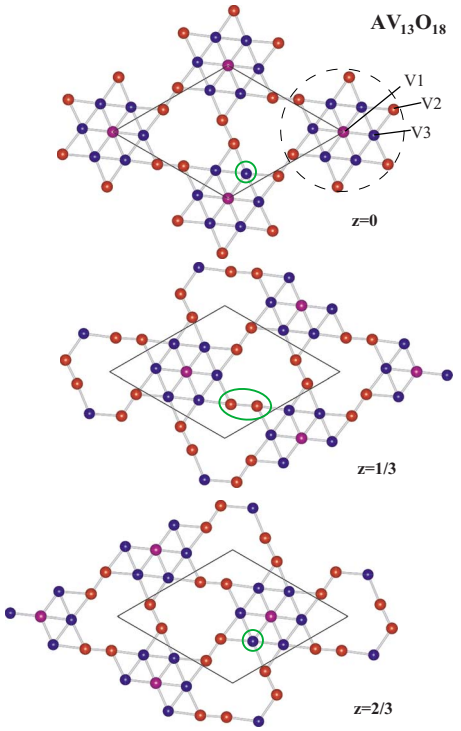

FIG. 1. (Color online) Arrangement of the V ions in $AV_{13}O_{18}$ at the $z=0$, 1/3, and 2/3 layer. The solid rhombi represent the unit cell in the hexagonal setting of the trigonal symmetry. The V ions surrounded by a solid circle or ellipsoid belong to the same tetramer, as an example of the formation of tetramers (see text). The figures of the crystal structure in the present paper were drawn by VESTA (Ref. 9).

position of the O ion. Therefore, $AV_{13}O_{18}$ can be regarded as VO in the sodium-chloride structure from which V and O ions are periodically missing and some O ions are replaced by the A ions.

The average valence of V in $AV_{13}O_{18}$ is $+2\frac{8}{13}$. This means that there are 31 electrons in total for 13 V ions.

II. EXPERIMENT

Polycrystalline samples of $SrV_{13}O_{18}$, $BaV_{13}O_{18}$ were synthesized by a solid-state reaction. Starting materials are $Sr_2V_2O_7$, V_2O_3, and V for $SrV_{13}O_{18}$ and $BaCO_3$, V_2O_3, and V for $BaV_{13}O_{18}$. These materials were mixed, pressed, and sintered. It was found that the $AV_{15}O_{15}$ phase appears if they are sintered at relatively low temperatures ($\sim$1300 °C) and once they are molten, $AV_{15}O_{15}$ also appears. Thus, we prepared a rod and sintered in the floating-zone furnace slightly below the melting point in the flow of forming gas (H_2 7% and Ar gas) with slowly moving the rod (0.5 mm/h).

Electrical-resistivity measurement was made by a four-probe technique. Magnetic susceptibility was measured by a superconducting quantum interference device magnetometer. Electron-diffraction experiment was carried out in a JEM-2010 transmission electron microscope operating at 200 kV. Synchrotron x-ray powder-diffraction measurement was performed with an incident wavelength of 0.7776 Å at SPring-8 BL02B2.[10] Rietveld analysis of the diffraction data was made with RIETAN-2000.[11]

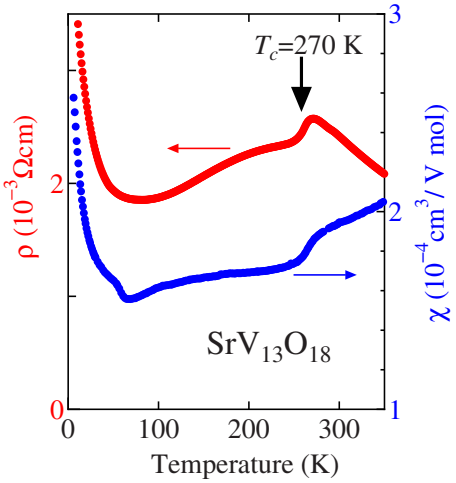

FIG. 2. (Color online) Temperature dependence of resistivity and magnetic susceptibility for $SrV_{13}O_{18}$.

III. RESULT

Figure 2 shows the T dependence of electrical resistivity (ρ) and magnetic susceptibility (χ) for $SrV_{13}O_{18}$. As can be seen, there is an anomaly at T_c=270 K in both $\rho(T)$ and $\chi(T)$. The $\rho(T)$ increases with decreasing T above T_c but exhibits a sharp decrease at T_c, and further decreases below T_c, indicating a metallic state below T_c in $SrV_{13}O_{18}$. There is an upturn in $\rho(T)$ at around 70 K. An anomaly at T_c =270 K is also observed in $\chi(T)$. There is another anomaly in $\chi(T)$ at 70 K, indicating spin ordering, whose nature has yet to be studied.

To understand the origin of the anomaly at T_c=270 K, we studied the crystal structure of $SrV_{13}O_{18}$ at various temperatures by synchrotron x-ray powder-diffraction measurement. We found that the crystal structure above T_c is consistent with that previously reported;[7,8] the space group is $R\bar{3}$. The lattice constants and the atomic parameters obtained by the Rietveld analysis of the diffraction data are summarized in the Appendix B. Below T_c, the splitting of the peaks and the appearance of new peaks were observed. An example is shown in Figs. 3(a) and 3(b). The 232 peak (in the hexagonal setting) is split into several peaks and new peaks, which can be assigned to $32\frac{7}{2}$ and $35\frac{1}{2}$, appear below T_c=270 K. Since the space group $R\bar{3}$ has only the threefold rotation (except for the inversion) as a symmetry operation, these results indicate the triclinic symmetry (the space group $P\bar{1}$) for the low T phase of $SrV_{13}O_{18}$. Furthermore, the appearance of hkl peak with half integer l indicates the doubling of the unit cell along the c direction. The primitive vectors of the high-T phase (both in the hexagonal and rhombohedral setting) and those of the low-T phase are shown in Fig. 4(a). The result of the Rietveld analysis of the x-ray diffraction data at 90 K based on such a structural model is shown in Fig. 3(c), and the obtained parameters are shown in the Appendix B. The

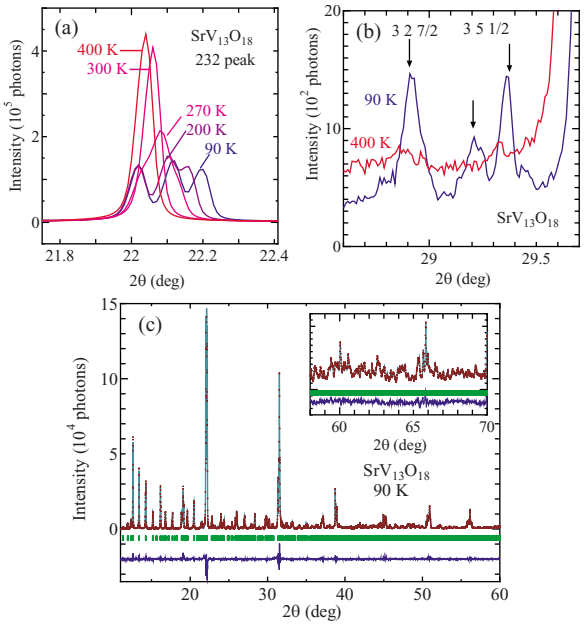

FIG. 3. (Color online) (a) Splitting of the 232 peak and (b) appearance of the $32\frac{7}{2}$ and $35\frac{1}{2}$ peaks in the synchrotron x-ray powder diffraction of $SrV_{13}O_{18}$. (c) Synchrotron x-ray powder-diffraction patterns (plus marks) and Rietveld refinement patterns (solid lines) of $SrV_{13}O_{18}$ at 90 K with $\lambda=0.7776$ Å. The vertical marks indicate the position of Bragg peaks and the solid line at the bottom corresponds to the difference between observed and calculated intensities. The inset is the expanded figure at higher angles $2\theta=60°-70°$.

temperature dependence of the lattice parameters (lengths and angles) is shown in Fig. 4(b).

According to the atomic positions obtained by the Rietveld analysis, there are short V-V bonds (<2.8 Å) and long V-V bonds (>2.8 Å) in this compound. Above T_c, short

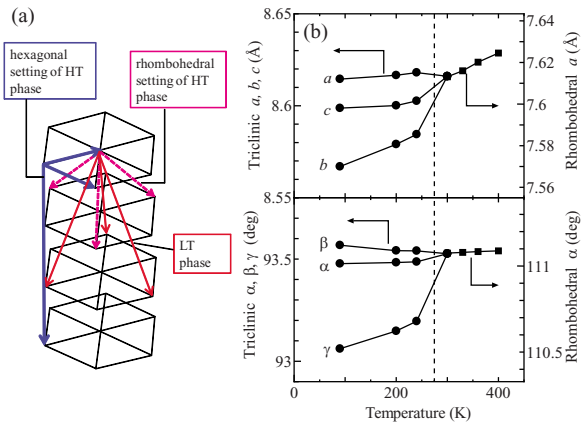

FIG. 4. (Color online) (a) Primitive vectors of the high-T (trigonal) phase (both in the hexagonal setting and rhombohedral setting) and those of the low-T (triclinic) phase for $SrV_{13}O_{18}$. (b) Lattice parameters, lengths (upper panel), and angles (lower panel), vs temperature for $SrV_{13}O_{18}$. The scales above $T_c=270$ K are given by the right axes and those below T_c are given by the left axes. The lattice parameters above T_c (trigonal phase) are defined in the rhombohedral setting.

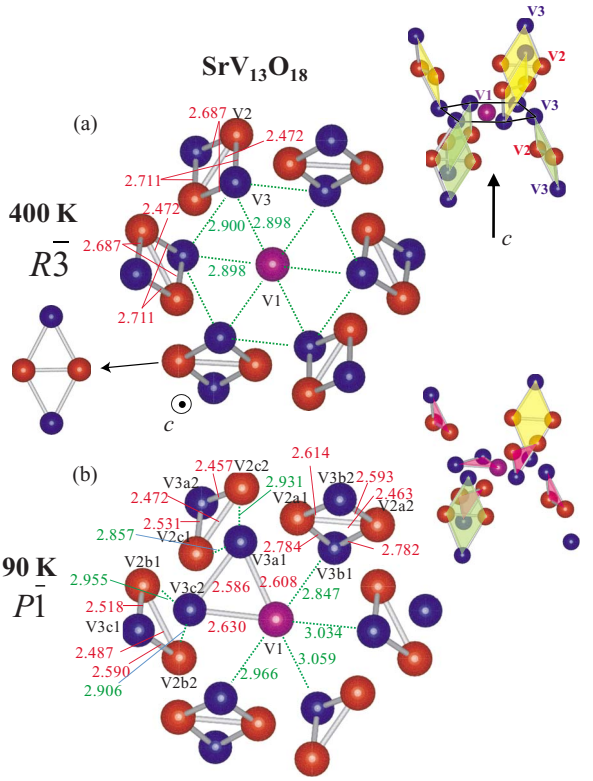

FIG. 5. (Color online) [(a) and (b)] Arrangement of V ions and the V-V bond lengths in angstrom for $SrV_{13}O_{18}$ seen from the c axis (in the hexagonal setting of the high-T phase) (a) at 400 K$>T_c$ and (b) at 90 K$<T_c$. A typical error of the bond length is ±0.006 Å. Thick bars connecting two V ions correspond to the short V-V bonds (<2.8 Å). The upper-right panels in (a) and (b) show the arrangement of the V ions seen from the direction perpendicular to the c axis.

V-V bonds form a V *tetramer*, which is composed of two parallel (quasi) regular triangles connected at their sides, as shown in Fig. 5(a). The center V ion of the "star" (V1) is surrounded by six tetramers, each of which is composed of one V ion at the same z layer (V3), two V ions at the next z layer (V2), and one V ion at the second next z layer (V3). In other words, one tetramer extends over three layers. The four V ions to form one tetramer are shown also in Fig. 1 by solid circles and ellipsoid. As shown in the upper-right panel of Fig. 5(a), six tetramers point upward or downward alternately around V1. In this structure, 13 V ions can be separated into one V at the center and three V tetramers.

Below T_c, the center V ion (V1) form a V *trimer* with two V3 ions on the same z layer, as shown in Fig. 5(b). Since these two V3 ions are taken from two tetramers, these two tetramers change into two trimers extending over two layers. Therefore, 13 V ions are separated into three trimers (one along a layer, and two extending over two layers) and one remaining tetramer (extending over three layers) in the low-T phase. It should be noted that the triangle of the in-plane trimer points to the opposite direction in the V star between the neighboring layers, as shown in Fig. 6(a), and this give rise to the doubling of the unit cell along the c direction. Namely, the direction of the trimers in the first layer is different from that in the fourth layer.

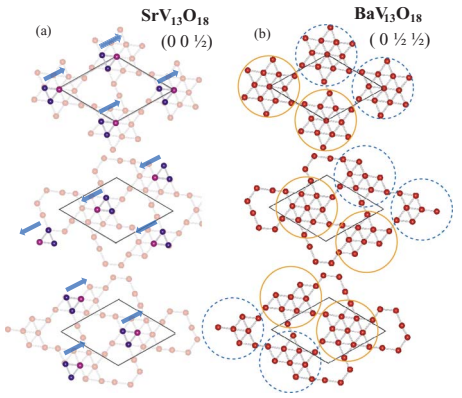

FIG. 6. (Color online) (a) Directions of the in-plane trimers at each z layer in $SrV_{13}O_{18}$. (b) A model of the low-T phase in $BaV_{13}O_{18}$. The star (composed of 13 V ions) surrounded by a solid circle and that by a dashed circle are inequivalent.

As discussed in the introduction, the V ions in $AV_{13}O_{18}$ is on the fcc lattice. Figure 7 shows an illustration of V tetramers and V trimers on the fcc lattice above and below T_c. One V trimer is composed of one V ion at the corner and two at the face center on the fcc lattice whereas one V tetramer is composed of one at the corner and three at the face center. By defining the z layer in Fig. 1 as the (111) plane in Fig. 7, the six tetramers (three inequivalent ones) surrounding the center V1 above T_c, is either along the $(11\bar{1})$, $(1\bar{1}1)$, or $(\bar{1}11)$ plane. Below T_c, one tetramer [$(1\bar{1}1)$ in this figure)] survives and the three trimers are either along the (111), $(11\bar{1})$, or $(\bar{1}11)$ plane.

Figure 8 shows the T dependence of electrical resistivity ρ and magnetic susceptibility χ for $BaV_{13}O_{18}$. There is an anomaly at T_c=200 K in both $\rho(T)$ and $\chi(T)$. The difference from $SrV_{13}O_{18}$ in $\rho(T)$ is that ρ critically increases at T_c and keeps increasing with decreasing T below T_c in $BaV_{13}O_{18}$, indicating an insulating character of the low-T phase.

We also studied the crystal structure of $BaV_{13}O_{18}$ by synchrotron x-ray powder-diffraction measurement. However, we could not find a drastic change in the crystal structure as observed in $SrV_{13}O_{18}$, except for a small change in the lattice constants at T_c as shown in Figs. 9(a) and 9(b). However, we

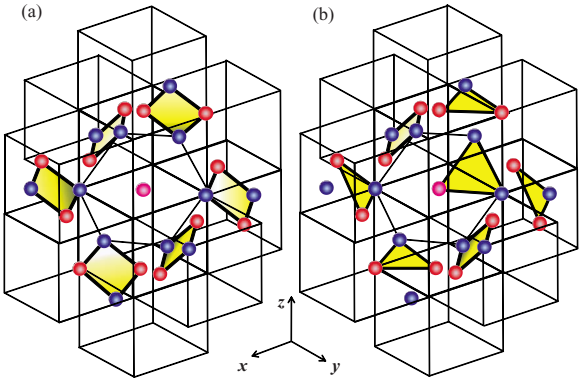

FIG. 7. (Color online) [(a) and (b)] Illustration of the V ions, V tetramers, and V trimers in $SrV_{13}O_{18}$ on the fcc lattice (a) above T_c and (b) below T_c.

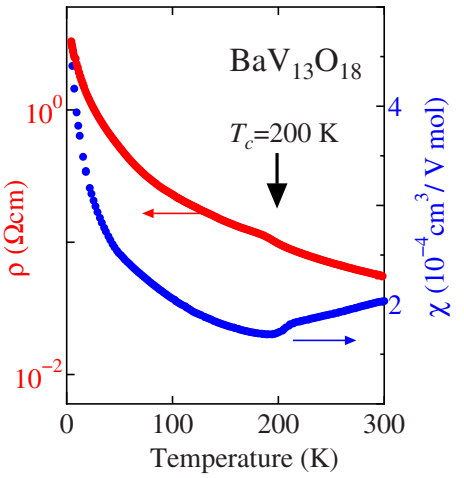

FIG. 8. (Color online) Temperature dependence of resistivity and magnetic susceptibility for $BaV_{13}O_{18}$.

observed superlattice peaks in the electron diffraction for (hkl) with half integer k and l below T_c, as shown in Fig. 9(c). One possible model of the low-T phase in $BaV_{13}O_{18}$ that is consistent with the experimentally observed superlattice peak at $0\frac{1}{2}\frac{1}{2}$ is shown in Fig. 6(b). Here, the 13V stars surrounded by a solid line and a dashed line become inequivalent, possibly due to the different valence of the V ions between two stars. This model suggests a charge-ordered state below T_c, consistent with the insulating behavior of resistivity. However, the electronic and orbital states of the low-T phase in $BaV_{13}O_{18}$ has yet to be clarified.

IV. DISCUSSION

First, let us consider the electronic structure of the V tetramer above T_c based on the idea of the orbital ordering in

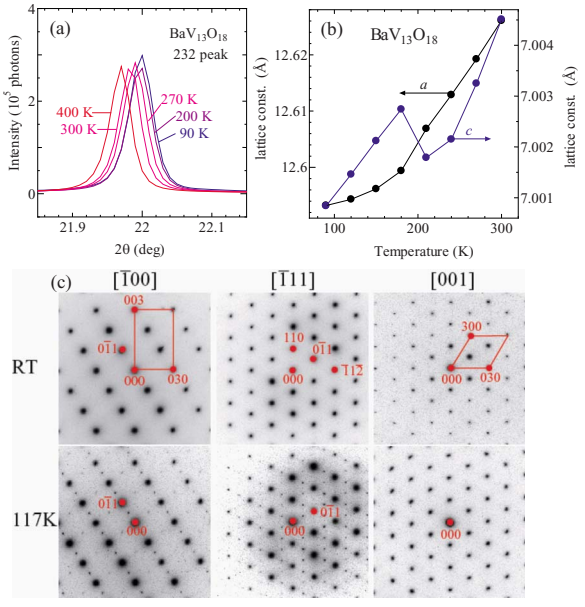

FIG. 9. (Color online) (a) The 232 peak in the x-ray diffraction pattern for $BaV_{13}O_{18}$. (b) Temperature dependence of lattice constants (in the hexagonal setting) for $BaV_{13}O_{18}$. (c) Electron-diffraction patterns of $BaV_{13}O_{18}$ above and below T_c=200 K taken from various directions.

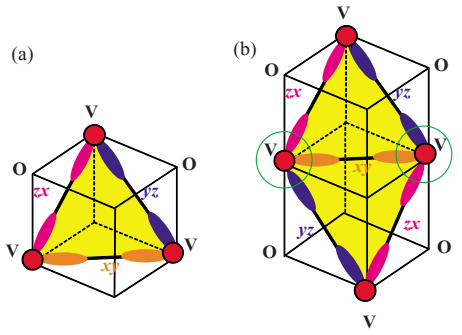

FIG. 10. (Color online) Orbital states of (a) a trimer and (b) a tetramer. The V ions surrounded by circles are those in which all the three t_{2g} states are used for the bond formation.

the V trimer of $LiVO_2$. As discussed in the introduction, xy, yz, or zx states form a bond at each side of the V triangles in such a trimer, as shown in Fig. 10(a), and six electrons can be accommodated in the three bonding states of a V trimer.[2] In a similar way, the orbital state in the tetramer of $SrV_{13}O_{18}$ can be constructed as shown in Fig. 10(b). There are five bonds, composed of either xy, yz, or zx orbitals, and thus, ten electrons can be accommodated in one tetramer in a spin-singlet state. This spin-singlet model is consistent with the substantially smaller value of magnetic susceptibility at room temperature, $\sim 2\times 10^{-4}$ cm^3/V mol for both Ba and Sr, compared with those of other vanadates with V^{3+} ions, for example, $\sim 1.5\times 10^{-3}$ cm^3/V mol for MgV_2O_4.[12] Furthermore, the temperature dependence of magnetic susceptibility above T_c shown in Figs. 2 and 8, i.e., $d\chi/dT>0$, is also a typical behavior of χ in the spin-singlet state, which is dominated by the thermally induced spin-triplet excitations. In this high-T phase above T_c, the 13 V ions in a unit cell are separated into three tetramers and one center V ion (V1), and three tetramers can accommodate 30 electrons. As discussed in the introduction, there are $31d$ electrons in 13 V ions in $AV_{13}O_{18}$, and thus, there is one d electron left in the center V1 ion, indicating that the V1 ion is V^{4+} $(3d^1)$.

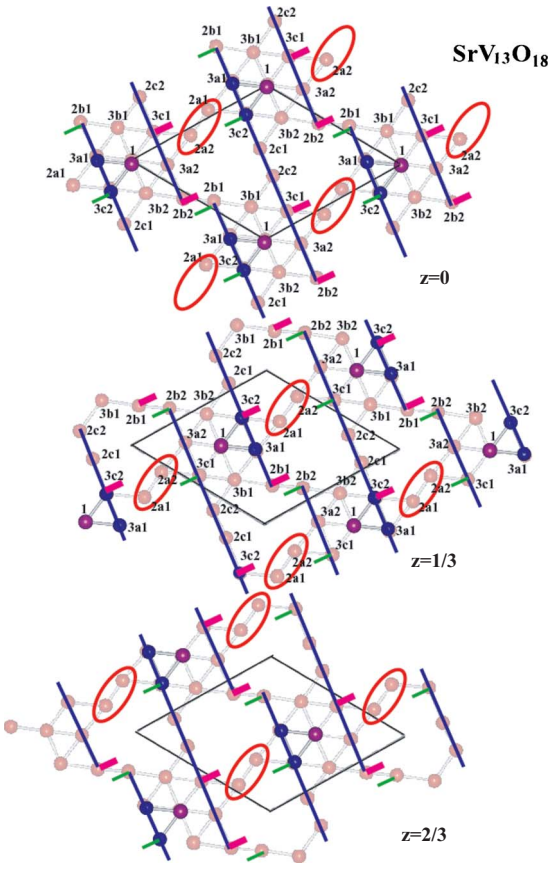

FIG. 11. (Color online) V lines composed of eight V ions (V2b2, V3a2, V3c1, V2c2, V2c1,V3c2, V3a1, and V2b1) are shown by blue solid long lines. The short lines indicate the connection between two lines on the adjacent layers; thick magenta lines indicate the connection to the upper layer, and the thin green lines to the lower layer. The ions surrounded by ellipsoids are bottlenecks of the electron transfer; the V ions in which all the three t_{2g} states are used for the bond formation.

In the low-T phase of $SrV_{13}O_{18}$, 13 V ions are separated into three trimers and one tetramer. Since one trimer can accommodate six electrons, $6\times 3+10=28$ electrons can be accommodated in total, and thus three electrons are left (not accommodated in trimers or tetramers) in this model.

As shown in the last section, resistivity sharply *decreases* at T_c with decreasing temperature in $SrV_{13}O_{18}$. Furthermore, $d\rho/dT$ is negative in the high-T phase, indicating a poorly conducting state but $d\rho/dT$ is positive in the low-T phase, indicating a metallic state. This is counterintuitive since the crystal is more distorted in the low-T phase. One possible origin of the poorly conducting state in the high-T phase is the two V ions in the tetramer [surrounded by circles in Fig. 10(b)], in which all the three t_{2g} states are used for the bond formation and thus occupied by electrons. In this situation, electrons cannot go through this V site unless they go on the antibonding state with higher energy. In the high-T phase, all the V2 ions (at the pointed tips of the star) are such ions and act as "bottlenecks" of electron transfer. In other words, the electron on the V1 site (the center of the star) cannot reach the V1 site in the neighboring unit cell (either on the same z layer or on the next layer) without going through the V2 sites (see Figs. 1 and 5). We speculate that such bottlenecks of the electron transfer at the V2 ions are the origin of the poorly conducting behavior in the high-T phase.

On the other hand, in the low-T phase of $SrV_{13}O_{18}$, two out of three tetramers are changed into trimers, and as a result, the number of the bottlenecks of the electron transfer is reduced (Fig. 11, where the remaining bottlenecks are shown by ellipsoids). Furthermore, we noticed that there is a unique characteristic in the crystal structure of the low-T phase; all the V ions in the three trimers except for one V ion (V1), i.e., eight V ions (V2b2, V3a2, V3c1, V2c2, V2c1,V3c2, V3a1, and V2b1), are aligned in straight without disturbed by the bottleneck as shown by the solid lines in Fig. 11. In addition, a line on one layer ($z=0$, for example) is connected to another line in the next layer ($z=1/3$), as shown by short thick lines in Fig. 11 and thus, the lines are infinitely connected. We speculate that the transfer of the remaining electrons along these lines, i.e., the band formation, is the origin of the metallic behavior in the low-T phase of $SrV_{13}O_{18}$.

V. SUMMARY

We studied the temperature dependence of resistivity, magnetic susceptibility, and the crystal structure of $SrV_{13}O_{18}$ and $BaV_{13}O_{18}$. It was found that both compounds exhibit a phase transitions at T_c=270 K (Sr) and T_c=200 K (Ba), where resistivity and magnetic susceptibility show anomalies. For $SrV_{13}O_{18}$, there is a structural phase transition at T_c=270 K from a trigonal to a triclinic phase, and the structural change is characterized by "three V tetramers and one V ion" in the high-T phase to "three V trimers and one V tetramers" in the low-T phase. The metallic behavior in the low-T phase of $SrV_{13}O_{18}$ can be explained by the itinerant band composed of eight V ions in a straight line. On the other hand, $BaV_{13}O_{18}$ shows an insulating behavior in the low-T phase, where superlattice peaks at $0\frac{1}{2}\frac{1}{2}$ were observed.

ACKNOWLEDGMENTS

We thank T. Okuda for useful discussion. This work was partly supported by Grant-in-Aids for Scientific Research on Priority Areas (Grant No. 20046014) from MEXT and Scientific Research B (Grant No. 21340105) from JSPS of Japan. The synchrotron-radiation experiments were performed at the BL02B2 in the SPring-8 with the approval of the Japan Synchrotron Radiation Research Institute (JASRI) (Proposal No. 2009B1068).

APPENDIX A: POSSIBLE ORBITAL STATES IN THE LOW-T PHASE OF $SrV_{13}O_{18}$

Let us discuss the orbital state in the low-T phase of $SrV_{13}O_{18}$ in more details. In Fig. 12, we plot the V lines (blue thick dashed lines), which are shown by the solid lines in Fig. 11 in the main text, on the fcc lattice. The left and right with the inversion relation correspond to the V lines on the neighboring layers in Fig. 11. In this figure, the electron transfer along the line occurs with the hybridization of the yz states at the neighboring V ions. Furthermore, the electron transfer between the two lines in the adjacent layers also occurs with the hybridization of the yz states. This means that the yz states form a quasi-one-dimensional "band" in the crystal.

This band formation seemingly has a problem since the yz states of some V ions have already been used for the bond formation of the trimers. For example, between V3c2 and V3a1, the yz states form a bond, and thus cannot be used for the yz band formation above. So far, we have taken account of only the direct d-d transfer between neighboring V ions but by taking account of the electron transfer between neighboring V sites through an O $2p$ state, we can escape from this problem. Namely, among three bonds in a trimer, one bond can be replaced with a bond composed of a supertransfer through an O $2p$ state. In the left panel of Fig. 13, as an example, the bond at the upper-right side of the triangle, which is supposed to be composed of the yz states by a d-d direct transfer, is now composed of the xy state and the zx state by a supertransfer through an oxygen $2p$ state. A characteristic of this trimer formation is that the same state (the yz state in Fig. 13) at all the three V ions is unoccupied. On

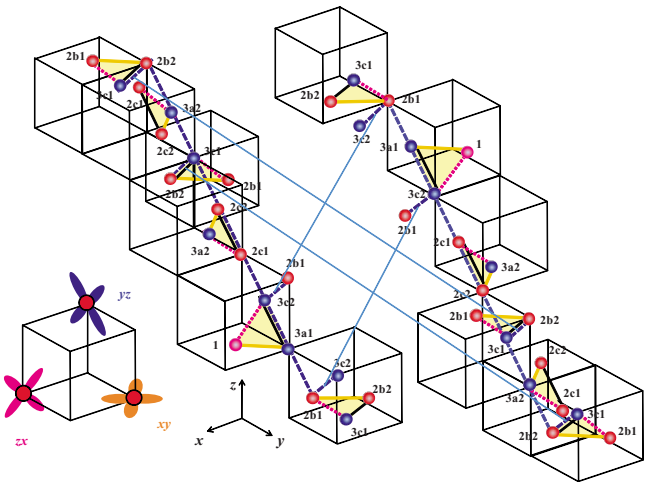

FIG. 12. (Color online) Illustration of the V lines composed of eight V ions (V2b2, V3a2, V3c1, V2c2, V2c1,V3c2, V3a1, and V2b1) on the fcc lattice. Left and right are those on adjacent layers, and have an inversion relation. The blue thick dashed lines indicate the hybridization network of the yz states for the band formation. The orange thick solid lines correspond to the bond by the xy states (d-d transfer). The magenta dotted lines correspond to the bond by the zx states (d-d transfer). The black thin solid lines correspond to the bond by the V-O-V supertransfer. Thin blue lines connect the equivalent bonds between two V lines.

the basis of the trimer shown here, the yz states at all the eight V ions on the line can be made unoccupied, and thus, as illustrated by the right panel of Fig. 13, the yz band can be formed along the line.

In Fig. 12, the orbital states on the line based on the model above are shown. The orange thick solid lines correspond to the bond by the xy states (d-d transfer), the magenta dotted lines to the bond by the zx states (d-d transfer), the black thin solid lines to the bond by the supertransfer, and the blue thick dashed lines to the hybridization of the yz states for the band formation. Note that a bond here means

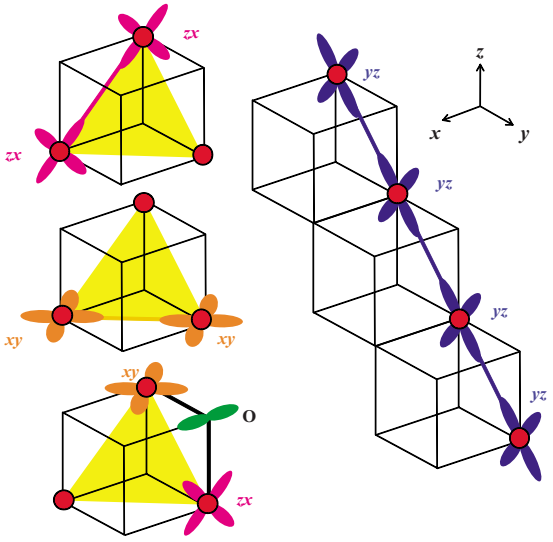

FIG. 13. (Color online) Orbital states of the bond on the trimer (left) and the band (right).

TABLE I. Atomic parameters of $BaV_{13}O_{18}$ at 300 K from the Rietveld analysis of the synchrotron x-ray powder-diffraction data. R_{wp}=6.78% and R_e=3.33%.

300 K, $R\bar{3}$

a (Å) 12.6261(1), c (Å) 7.00451(6)

Atom (site)	x	y	z	B (Å^2)
Ba (3a)	0	0	0	0.48(3)
V1 (3b)	0	0	1/2	0.21(7)
V2 (18f)	0.0505(2)	0.4367(2)	0.5032(4)	0.14(3)
V3 (18f)	0.4906(2)	0.9318(2)	0.1771(3)	0.24(3)
O1 (18f)	0.4763(7)	0.7932(6)	0.005(1)	0.79(5)
O2 (18f)	0.1694(6)	0.4080(5)	0.658(1)	0.79(5)
O3 (18f)	0.0350(6)	0.2899(7)	0.340(2)	0.79(5)

TABLE II. Atomic parameters of $BaV_{13}O_{18}$ at 90 K from the Rietveld analysis of the synchrotron x-ray powder-diffraction data. R_{wp}=6.16% and R_e=2.84%.

90 K, $R\bar{3}$

a (Å) 12.5932(2), c (Å) 7.00084(7)

Atom (site)	x	y	z	B (Å^2)
Ba (3a)	0	0	0	0.12(3)
V1 (3b)	0	0	1/2	0.24(7)
V2 (18f)	0.0505(2)	0.4372(2)	0.5015(4)	0.00(3)
V3 (18f)	0.4898(2)	0.9313(2)	0.1781(3)	0.14(3)
O1 (18f)	0.4770(7)	0.7934(6)	0.007(1)	0.67(5)
O2 (18f)	0.1702(6)	0.4100(5)	0.659(1)	0.67(5)
O3 (18f)	0.0333(6)	0.2901(7)	0.334(2)	0.67(5)

TABLE III. Atomic parameters of $SrV_{13}O_{18}$ at 400 K from the Rietveld analysis of the synchrotron x-ray powder-diffraction data. R_{wp}=7.75% and R_e=2.85%.

400 K, $R\bar{3}$

a (Å) 12.5747 (1), c (Å) 6.99328 (6)

Atom (site)	x	y	z	B (Å^2)
Sr (3a)	0	0	0	0.95(6)
V1 (3b)	0	0	1/2	0.32(7)
V2 (18f)	0.0507(1)	0.4375(1)	0.5029(2)	0.21(2)
V3 (18f)	0.4898(2)	0.9312(2)	0.1770(2)	0.42(3)
O1 (18f)	0.4742 (5)	0.7909(4)	0.0026(6)	0.59(3)
O2 (18f)	0.1711(4)	0.4105(4)	0.660(1)	0.59(3)
O3 (18f)	0.0352(5)	0.2901(5)	0.3424(8)	0.59(3)

TABLE IV. Atomic parameters of $SrV_{13}O_{18}$ at 90 K from the Rietveld analysis of the synchrotron x-ray powder-diffraction data. R_{wp}=9.35% and R_e=3.89%. The Debye-Waller factors B of the V and O were set to 0.1 in the analysis.

90 K, $P\bar{1}$

a (Å) 8.61452(8), b (Å) 8.56697(8), c (Å) 8.59874(8), α (deg) 93.4777(6), β (deg) 93.5679(6), γ (deg) 93.0612(6)

Atom (site)	x	y	z	B (Å^2)
Sr1 (1a)	0	0	0	0.06(4)
Sr2 (1h)	1/2	1/2	1/2	0.06(4)
V1 (2i)	0.7636(6)	0.7472(6)	0.7417(6)	0.1
V2a1 (2i)	0.1846(6)	0.7042(6)	0.3685(6)	0.1
V2a2 (2i)	0.6904(6)	0.1970(6)	0.8586(6)	0.1
V2b1 (2i)	0.8576(5)	0.6785(6)	0.1895(6)	0.1
V2b2 (2i)	0.3729(6)	0.1986(6)	0.7065(6)	0.1
V2c1 (2i)	0.2112(5)	0.8813(6)	0.6929(6)	0.1
V2c2 (2i)	0.6910(6)	0.3514(5)	0.1844(6)	0.1
V3a1 (2i)	0.0043(5)	0.6084(5)	0.6426(6)	0.1
V3a2 (2i)	0.5295(6)	0.1046(5)	0.1496(6)	0.1
V3b1 (2i)	0.1438(6)	0.5140(6)	0.0942(6)	0.1
V3b2 (2i)	0.6504(6)	0.0303(6)	0.5969(6)	0.1
V3c1 (2i)	0.6044(6)	0.6437(6)	0.0266(6)	0.1
V3c2 (2i)	0.0936(6)	0.1549(5)	0.4985(6)	0.1
O1a1 (2i)	0.790(2)	0.527(2)	0.680(2)	0.1
O1a2 (2i)	0.295(2)	0.035(2)	0.186(2)	0.1
O1b1 (2i)	0.692(2)	0.798(2)	0.525(2)	0.1
O1b2 (2i)	0.175(2)	0.282(2)	0.031(2)	0.1
O1c1 (2i)	0.540(2)	0.687(2)	0.794(2)	0.1
O1c2 (2i)	0.019(2)	0.163(2)	0.277(2)	0.1
O2a1 (2i)	0.231(2)	0.674(2)	0.597(2)	0.1
O2a2 (2i)	0.739(2)	0.147(2)	0.078(2)	0.1
O2b1 (2i)	0.096(2)	0.742(2)	0.150(2)	0.1
O2b2 (2i)	0.583(2)	0.250(2)	0.659(2)	0.1
O2c1 (2i)	0.659(2)	0.573(2)	0.248(2)	0.1
O2c2 (2i)	0.158(2)	0.115(2)	0.730(2)	0.1
O3a1 (2i)	0.962(2)	0.638(2)	0.429(2)	0.1
O3a2 (2i)	0.461(2)	0.127(2)	0.911(2)	0.1
O3b1 (2i)	0.425(2)	0.967(2)	0.636(2)	0.1
O3b2 (2i)	0.906(2)	0.455(2)	0.131(2)	0.1
O3c1 (2i)	0.140(2)	0.925(2)	0.464(2)	0.1
O3c2 (2i)	0.631(2)	0.411(2)	0.960(2)	0.1

that hybridization of a state occurs only with a single neighboring site (xy and zx states in Figs. 12 and 13) whereas a band is formed when hybridization occurs with more than two neighboring sites (yz states in Figs. 12 and 13). Therefore, the electronic states of the low-T phase in $SrV_{13}O_{18}$ proposed here can be regarded as the coexistence of the bonds localized on the trimers and the band extending in the crystal.

As discussed in the main text, three electrons in 13 V ions are left after the trimer formation and those three should be accommodated in the *yz* band. This odd number indicates a metallic state. However, because of the doubling of the unit cell (which corresponds the existence of two V lines in the opposite direction shown in Fig. 12), there are six electrons in the band and the state can be insulating. Indeed, a preliminary result of the Hall measurement indicates a small number of carriers at the lowest temperature (~0.01 electron per V) and a large T dependence. These features suggest a semimetallic state in the low-T phase of $SrV_{13}O_{18}$. Namely, there are a small number of electrons and holes with different relaxation times. This situation is possible when six electrons exist in the band.

APPENDIX B: STRUCTURAL PARAMETERS

Structural parameters obtained by the Rietveld analysis for $BaV_{13}O_{18}$ at 300 K ($>T_c$=200 K) and 90 K ($<T_c$) and for $SrV_{13}O_{18}$ at 400 K ($>T_c$=270 K) and 90 K ($<T_c$) are listed in Tables I–IV.

*Author to whom correspondence should be addressed.

[1] Y. Murakami *et al.*, Phys. Rev. Lett. **81**, 582 (1998).
[2] H. F. Pen, J. van den Brink, D. I. Khomskii, and G. A. Sawatzky, Phys. Rev. Lett. **78**, 1323 (1997).
[3] J. Miyazaki, T. Sonehara, D. Akahoshi, H. Kuwahara, J. E. Kim, K. Kato, M. Takata, and T. Katsufuji, Phys. Rev. B **79**, 180410(R) (2009).
[4] C. A. Bridges and J. E. Greedan, J. Solid State Chem. **177**, 1098 (2004).
[5] T. Kajita, T. Kanzaki, T. Suzuki, J. E. Kim, K. Kato, M. Takata, and T. Katsufuji, Phys. Rev. B **81**, 060405(R) (2010).
[6] J. Miyazaki, K. Matsudaira, Y. Shimizu, M. Itoh, Y. Nagamine, S. Mori, J. E. Kim, K. Kato, M. Takata, and T. Katsufuji, Phys. Rev. Lett. **104**, 207201 (2010).
[7] K. Iwasaki, H. Takizawa, K. Uheda, T. Endo, and M. Shimada, J. Solid State Chem. **158**, 61 (2001).
[8] K. Iwasaki, H. Takizawa, H. Yamane, S. Kubota, J. Takahashi, K. Uheda, and T. Endo, Mater. Res. Bull. **38**, 141 (2003).
[9] K. Momma and F. Izumi, J. Appl. Crystallogr. **41**, 653 (2008).
[10] E. Nishibori, M. Takata, K. Kato, M. Sakata, Y. Kubota, S. Aoyagi, Y. Kuroiwa, M. Yamakata, and N. Ikeda, Nucl. Instrum. Methods Phys. Res. A **467-468**, 1045 (2001).
[11] F. Izumi and T. Ikeda, Mater. Sci. Forum **321-324**, 198 (2000).
[12] H. Mamiya and M. Onoda, Solid State Commun. **95**, 217 (1995).